Tellus (1988), *40A*, 177–187

On the resonance of an external planetary wave and its interaction with the mean zonal flow

By PIERRE DIONNE,[1] HERSCHEL L. MITCHELL[2] and JACQUES DEROME,[1]
[1] *Department of Meteorology, McGill University, Montréal, Québec, Canada H3A 2K6,* [2] *Recherche en prévision numérique, Atmospheric Environment Service of Canada, Dorval, Québec, Canada H9P 1J3*

(Manuscript received 8 January 1987; in final form 28 August 1987)

ABSTRACT

Numerical experiments are performed to examine the resonant growth of a topographically forced wave in a nonlinear model. Time-dependent simulations are made including damping mechanisms, wave–mean flow interactions, a zonal wind driving force and wave–wave interactions. The initial mean zonal wind permits the resonance of the barotropic mode, rather than the first internal mode as in a previous study. It is found that even when damping and nonlinear interactions are included, the growth rate and the amplitude achieved by the resonant barotropic wave are similar to those occurring in observed planetary wave amplification episodes, such as those seen in some developing blocking conditions. Eliassen–Palm flux cross-sections of one of the integrations are presented to illustrate the interaction between the forced wave and the mean zonal flow.

1. Introduction

Although the importance of resonance effects in forced steady-state models of the atmosphere is widely recognized (see, e.g., Held (1983)) their influence in time-dependent models is less often discussed. In a recent study, Mitchell and Derome (1985), hereafter referred to as MD85, examined the resonant growth of a topographically forced wave in a nonlinear model. Their work was largely motivated by the proposal (see, e.g., Tung and Lindzen (1979)) that atmospheric blocking patterns may be the result of a resonant amplification of forced large-scale waves, but the tropospheric resonant growth rates that they obtained, were rather small compared with those observed in developing blocks. In addition the model underwent a stratospheric warming and a zonal wind reversal which threw the system off resonance before a large forced wave amplitude could be achieved in the troposphere. The low tropospheric growth rates were ascribed to the fact that the initial mean zonal wind led to the resonance of the first internal mode of the model rather than the external mode. Analytical results with simple zonal wind structures show that the external mode, which Tung and Lindzen (1979) showed to have *linear* growth rates comparable to those observed during a particular planetary wave amplification episode, will have larger tropospheric growth rates than the internal modes (see, e.g., Mitchell (1982), eq. (2.23)).

In the present paper we examine the resonant growth of a topographically forced wave by means of a nonlinear model, as in MD85, except that we use an initial mean zonal wind structure more conducive to resonating the external mode. As suggested in MD85, at $t = 0$ the meridional profile of the mean zonal wind $\bar{u}$ is taken to be a constant plus a sinusoidal component. The parameters entering the analytic representation of $\bar{u}$ are chosen such as to yield reasonable horizontal and vertical profiles and resonance at the scale of the forcing. The search for the resonant $\bar{u}$ is performed with a linear, steady-state version of the model, but subsequent calculations are based on the time-dependent version. A linear form of the latter is first used to determine the resonant growth rate. Damping is then included and experiments are performed with both the linear and nonlinear versions of the model. Naturally, as the forced wave amplifies it extracts energy from the mean zonal flow; the interesting point is to see how large the resonant wave can grow before substantially modifying $\bar{u}$, thereby throwing the system off resonance. The results indicate that the amplification rate and the maximum amplitude that the wave reaches are quite comparable to those published by Tung and Lindzen (1979, Fig. 2) and Austin (1980, Fig. 14).

Recently Hansen (1986) and Sutera (1986) have examined the Northern Hemisphere 500 mb height fields for the 4 winters from 1980–81 to 1983–84. In particular they studied the wavenumber band 2–4, which comprises those waves that according to Rossby's formula could become stationary for observed zonal winds. They found that the amplitude of these waves for each winter separately and for all winters combined exhibits a definite bimodal distribution. One mode, which they denoted Mode 1, is rather zonal in appearance, while the other mode, denoted Mode 2, exhibits amplified planetary waves with a pronounced ridge over the western coast of North America and deep troughs over the western Pacific Ocean and eastern North America. Austin (1980) has argued that blocking episodes can be explained by interference patterns of stationary planetary waves having normal phases but unusually large amplitudes, while Sutera (1986) has argued that blocking events correspond to the Mode 2 flow configuration just as periods of predominantly zonal flow fall into Mode 1. On the other hand, according to Hansen (1986), episodes of the spatially isolated characteristic flow pattern now called "Rex blocking" do not necessarily satisfy the criteria for inclusion in the Mode 2 category. In the present paper only a single zonal wavenumber is forced and achieves large amplitude. This study is therefore directed more towards the phenomenon of planetary wave amplification as it manifests itself in the Mode 2 configuration of Hansen (1986) and Sutera (1986) than to episodes of "Rex blocking".

The remainder of the paper is organized as follows. In Section 2 we present the numerical model which is then used, in Subsection 3.1, in a steady-state linear version in a search for the resonant mean zonal wind structures; in Subsection 3.2 the time-dependent version of the model is used to obtain the linear resonant growth rate. We then discuss the results of a nonlinear time integration in Section 4. Eliassen–Palm cross-sections are shown to illustrate the vertical propagation of the forced disturbance and its interaction with the mean zonal flow. Finally in Section 5 we present a summary of our results and our conclusions.

2. The numerical model

The model to be used is basically that described in MD85. It integrates the quasi-geostrophic potential vorticity equation on a beta-plane channel assumed to be of length L and to be bounded by rigid walls at $y = 0$ and $y = D$. A rigid lid is imposed at the upper boundary while the vertical velocity at the lower boundary incorporates the effects of both topographical forcing and Ekman pumping. The model also includes a Newtonian cooling term which tends to damp the eddies in the upper atmosphere and a Newtonian forcing term, which acts to force the zonal flow towards an externally specified profile. This latter term, which is intended to model the effect of radiative and diabatic processes on the zonal flow, will be included in the nonlinear time-dependent integration discussed in Section 4.

In the vertical, a log-pressure vertical coordinate, denoted Z, is employed. The vertical discretization uses finite differences with equal ΔZ increments. The horizontal discretization employs the spectral method. At any level k, the stream-function ψ is expanded as follows:

$$\psi(x, y) = -u_c y + \sum_{n=1}^{N} B_{0n} \cos \hat{n} y + \sum_{m=1}^{M} \sum_{n=1}^{N} [A_{mn} \sin \hat{m} x + B_{mn} \cos \hat{m} x] \sin \hat{n} y, \quad (1)$$

where

$$\hat{m} = m(2\pi/L) \quad \text{and} \quad \hat{n} = n\pi/D, \quad (2)$$

m and n being positive integers. Inclusion of the term $-u_c y$ in (1) is the only difference between the model employed in the present study and that described in MD85. This more general expansion, which allows the zonally averaged wind to equal a non-zero constant u_c at each boundary, was employed by Mitchell and Derome (1983). Its use here permits us to obtain an initial mean zonal wind structure for which the external mode is resonant. Kusunoki (1984) and MD85 have discussed how the $u_c y$ term in (1) affects the position of the resonance points in parameter space. Further details regarding the numerical aspects of this more general expansion can be found in Mitchell (1982, Appendix F).

To facilitate the comparison of our results with those of MD85, we will adopt as much as possible the same parameters used in that work. Thus L is taken to be the length of the latitude circle at 60°N and D is taken to be 40 degrees of latitude. We note that the zonal and meridional scales of our domain correspond to those modes which are found to be slowly moving in a spherical barotropic model linearized about a realistic zonal background state (Kasahara, 1980). These are the modes which are candidates for resonant amplification due to stationary forcing. The buoyancy frequency in the model is calculated using a constant value of temperature of 239°K. The topography is specified as

$$\hbar = \hbar_0 \sin(4\pi x/L) \sin(\pi y/D) \tag{3}$$

with $\hbar_0$ taken to be 500 m.

With the addition of a constant term to the mean zonal wind profile used by MD85, the mean zonal wind now has the following structure

$$\bar{u}(y, Z) = u_c + [u_0 + u_1 \operatorname{sech} \alpha(Z - Z_0)] \times \sin(\pi y/D). \tag{4}$$

Z_0 is set to 60 km and α is fixed at 0.658×10^{-4} m^{-1} to give a width of 40 km at half maximum. As in MD85, $\bar{u}(y, Z)$ has no tropospheric jet so that resonant growth can be examined without the simultaneous occurrence of baroclinic instability. The parameters u_c, u_0 and u_1 will be determined in Section 3.

The vertical profiles of both the Newtonian cooling and zonal flow forcing coefficients are as given in MD85. So too are the other parameters of the model; thus N, the number of functions retained in the meridional direction, is chosen to be 15, ΔZ is set to 3 km and a 24-level model is adopted.

3. The linear experiments

3.1. *Resonance in the steady-state model*

As in MD85, mean zonal wind profiles for which resonance occurs are found by defining a sequence of profiles $\bar{u}(y, Z)$ and for each profile solving for the linear steady-state response to the topographical forcing specified by (3). For a fixed zonal wavenumber m, the steady-state response magnitude R was defined as in MD85 by

$$R = \sum_{k=1}^{K} \exp(-Z_k/H) \sum_{n=1}^{N} [\hat{m}^2 + \hat{n}^2] \times [[A_{mn}^{(k)}]^2 + [B_{mn}^{(k)}]^2], \tag{5}$$

where Z_k is the height at level k, H is the scale height and $\hat{m}$, $\hat{n}$, $A_{mn}^{(k)}$ and $B_{mn}^{(k)}$ have been defined above.

In a first experiment, both u_c and u_0 were fixed at 8 m/s and R was calculated as u_1 was incremented by 1 m/s from 0 to 180 m/s. Throughout this parameter range, R was found to exceed 10^4 m^2/s^2 indicating (cf. MD85, Fig. 2) that for all these values of u_1 the response is very close to resonance. A single resonance peak was observed at $u_1 = 75$ m/s. Examination of the structure of the wave response indicated a resonant external mode.

This experiment was then repeated with the inclusion of both Ekman pumping and Newtonian cooling. Instead of the singular behaviour observed previously, R now varied very little (from 3.0×10^3 to 4.1×10^3 m^2/s^2) as u_1 was increased, because all of these wind profiles are so close to precise resonance. Since the external mode is trapped in the lower atmosphere, it was to be expected that in the presence of damping the resonance of this mode would exhibit very little sensitivity to the parameter u_1, which affects $\bar{u}$ more strongly in the stratosphere than in the lower troposphere, in agreement with the results of Salby (1981).

The value of R can, however, be expected to vary as the mean zonal wind structure changes in the lower atmosphere. Fig. 1 is a contour plot of R as a function of u_c and u_0 for u_1 fixed at 75 m/s. To produce the figure, the response in the presence of Ekman pumping and Newtonian cooling was calculated by increments of 0.5 m/s for the range of u_c and u_0 shown in the figure. The contouring routine used a cubic spline interp-

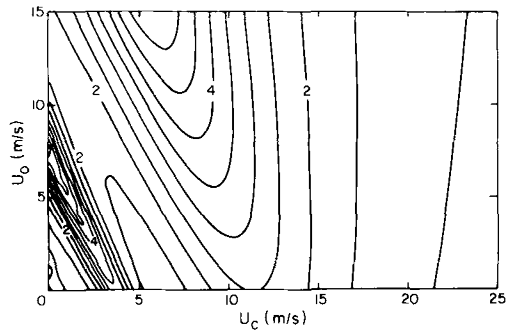

Fig. 1. The steady-state response magnitude (1000 m^2/s^2) as a function of u_c and u_0, with u_1 fixed at 75 m/s. 15 modes were used in the meridional direction and both Ekman pumping and Newtonian cooling were included.

olation to approximate the value of the response between the "grid points". Because of the rapidly increasing responses in the bottom left part of the diagram, this interpolation produced several wavy contour lines between the "grid points". However this region of the graph corresponds to the resonance of the first internal mode which will not be studied here. We can see a "ridge" of large amplitudes approximately following a line from $u_0 = 15$ m/s and $u_c = 6$ m/s to $u_0 = 0$ m/s and $u_c = 11$ m/s. The zonal wind profiles along that ridge are those for which the external mode is resonant. When damping is not included, resonance occurs at approximately the same values of u_0 and u_c, but because of the infinite response occurring at precise resonance, the "ridge" is replaced by a singular line.

On the basis of these results, the mean zonal wind profile defined by $u_c = u_0 = 8$ m/s and $u_1 = 75$ m/s will be adopted for use in the time-dependent integrations so that the external mode will be resonant.

3.2. *Resonance in the linear time-dependent model*

In these experiments $\bar{u}$ defined by (4) was kept constant in time and only wavenumber two, the forced wave, was permitted in the zonal direction. A time integration with initial wave amplitudes equal to zero showed the presence of large transients excited by the initial switch-on of the forcing. To reduce the amplitude of these transients we proceeded, as in MD85, to try to determine the steady-state amplitude of the non-resonant modes by calculating the time-average of the wave amplitudes in a linear integration of several months duration. These time-averaged amplitudes were then used in a subsequent integration as the initial values for the components having $\sin(4\pi x/L)$ dependence. The results of that integration showed a resonant barotropic wave growing linearly with time at the rate of approximately 10 dam per day throughout most of the model atmosphere (somewhat more slowly in the upper part). Comparing growth rates in the troposphere we note that this growth rate is more than an order of magnitude larger than that found by MD85 (Fig. 4) for a resonant first internal mode.

Next, the effects of Newtonian cooling and Ekman pumping were included. As in MD85, the initial conditions used to avoid exciting the transients in the inviscid integration were used to minimize the transients in the viscous integration. Fig. 2 shows the 30-day time-height cross-sections of the wave amplitude [scaled by $\exp(-Z/2H)$ and unscaled] at mid-channel. In the troposphere, the wave grows almost 50 dam in 10 days and reaches an equilibrium amplitude of about 55 dam. This growth rate and magnitude reached at equilibrium agree quite well with those calculated by Tung and Lindzen (1979, Fig. 2). Fig. 2b indicates that there are still transients, particularly in the upper atmosphere. Further

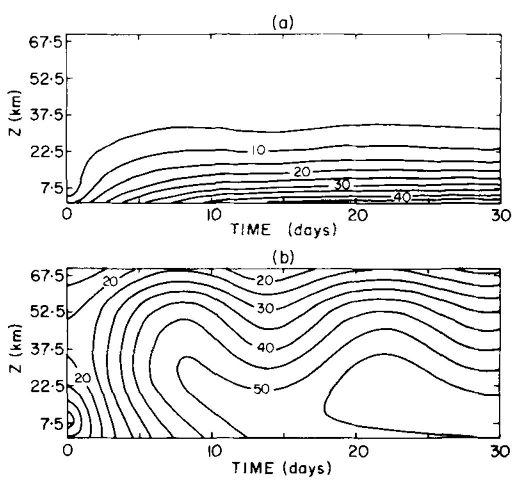

Fig. 2. Time–height cross-section of the wavenumber 2 height amplitude (dam) at mid-channel from the linear time integration with Ekman pumping and Newtonian cooling: (a) the scaled wave amplitude, (b) the unscaled wave amplitude.

examination reveals that the amplitudes of these transients range from slightly more than 5 dam in the upper model atmosphere to slightly less than 1 dam at the bottom of the model atmosphere. This is several times smaller than the amplitudes of the transients arising in a similar run done from zero amplitude initial conditions. In any case, the amplitude of the transients in our integration is quite small relative to the total wave amplitude and, as can be seen from Fig. 2a, the amount of energy associated with these transients is also small.

4. The nonlinear time-dependent experiment

We have seen in the previous experiment that, even in the presence of dissipation mechanisms, the wave amplitude grows to considerable amplitude, thus casting some doubt on the validity of the linear integration at large t. We therefore turn now to the results of the fully nonlinear model. To simulate the effects of the mean zonal diabatic processes in the atmosphere, we have included a Newtonian mechanism driving the mean zonal wind towards a structure $\bar{u}^*(y, Z)$ equal to $\bar{u}(y, Z, t = 0)$, computed with $u_c = u_0 = 8$ m/s and $u_1 = 75$ m/s. The relaxation coefficient implied in this term is that used by MD85. The relaxation time is approximately 7 days near the bottom of the domain and then increases to 23 days at 15 km, above which it follows the vertical profile used by Holton and Mass (1976). Zonal wavenumbers 2 to 10 were included in the calculations (because wavenumber 2 is forced, only the even zonal wavenumbers can be activated). As in the previous integrations, Newtonian cooling and Ekman pumping acted on the eddies and the initial conditions were chosen to minimize the excitation of transients.

We can visualize the time evolution of the flow from Figs. 3 and 4, which show zonal and horizontal sections through some variables. Fig. 3a is a time-height plot of the zonal wavenumber 2 amplitude at mid-channel. The amplitudes of the other waves are always very small and are not shown. We see that at the 10 km level, the wavenumber 2 amplitude grows from about 4 dam at day 0 to about 37 dam at day 8. Although we did not attempt to reproduce the exact atmospheric conditions of any particular observed

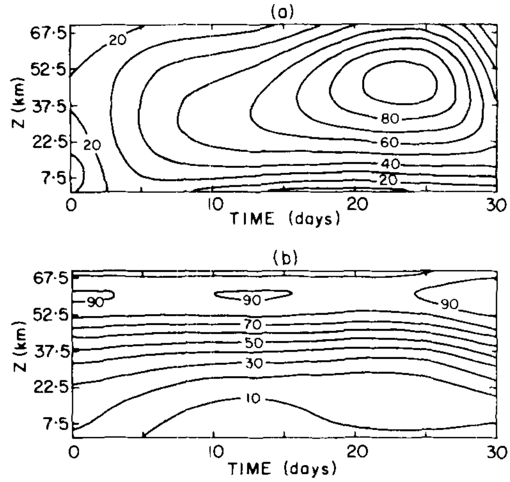

Fig. 3. (a) As in Fig. 2b but for the nonlinear integration. (b) Time-height cross-section of the mean zonal wind (m/s) at mid-channel.

planetary wave amplification, it is nevertheless of interest to note that our model produces a growth rate and achieves an amplitude similar to those published by Matsuno (1971, Fig. 3) for the observed amplification of zonal wavenumber 2 during January 1963 (based on data from Hirota; see also Tung and Lindzen, 1979, Fig. 2). In that case the amplitude of wavenumber 2 at 300 mb, 65° N, was observed to increase from 10 dam to 40 dam in about 10 days while we have seen that in our model the amplitude increases at a similar rate. Our model wave growth at 500 mb is also similar to that of another episode of planetary wave amplification discussed by Austin (1980, Fig. 14). The observed 500 mb wavenumber 2 grew by approximately 20 dam in 8 days while our results show a growth from about 5 to almost 30 dam during the first 8 days (see also Fig. 4). After day 8, our forced wave decays to an amplitude of about 15 dam at day 19 and then grows again. This time scale and general temporal behaviour is similar to that of the planetary wave amplitude indicator for the winter of 1981-82 presented by Hansen (1986, Fig. 6) and the zonal wavenumber 2 data presented by Matsuno, although the agreement may be fortuitous. The important point is that the initial growth rate and the amplitudes achieved in the troposphere are much larger than those achieved by the internal mode resonance of MD85. It is clear then that it is possible for a resonant wave to grow to considerable amplitude in the troposphere even when (1) the interaction with the mean zonal wind can throw the latter off resonance and (2) the strength of the wave forcing depends on the mean zonal wind speed.

We have verified that the restoring force acting on the mean zonal wind does not play a dominant role in our results. As zonal wavenumber two is the only significant wave, the model was rerun with only that harmonic interacting with the mean zonal wind and, more significantly, with no restoring force acting on the mean zonal flow. The forced wave results were similar to those shown in Fig. 3a. The main differences were that in the troposphere, from about day 5 onwards, the wave amplitude decayed slowly, whereas in Fig. 3a, a similar decay is followed by a weak growth after about day 20. In the upper levels, the wave maximum (approximately 103 dam) occurred a few kilometers higher and a few days later. We conclude that our main results are not strongly influenced by the mean zonal flow restoring force that we have used.

Fig. 3b shows a 30-day time–height cross-section of the zonal wind at mid-channel. The deceleration of the mean westerlies during the initial stages of the integration is evident, especially at the lower levels. This implies not only that the mean zonal wind moves off its resonant state, thereby reducing the response of the model to a given forcing, but also that the topographic wave forcing itself, which is proportional to $\bar{u}$ at $Z = 0$, is being reduced.

The behaviour of the zonal wind in the stratosphere is totally different from what was observed by MD85 in similar experiments with a resonant first internal mode. In their model, a reversal of the zonal wind took place at about day 10, followed by a return to westerlies roughly ten days later. In our experiment the mean zonal wind is westerly at all times. Holton and Mass (1976) found that there exists a critical value of forcing beyond which stratospheric vacillation cycles are observed and below which a more steady stratospheric circulation is established, a behaviour indicative of a bifurcation. Holton and Dunkerton (1978) subsequently reported that the critical forcing value depends strongly on $\bar{u}$. Since our mean zonal wind at $t = 0$ (and hence also our forcing) is stronger than that of MD85, the difference in the resulting behaviours could not be predicted on the basis of those papers. It would seem however that the first internal mode resonated by MD85's $\bar{u}(y, Z)$ structure, having a large amplitude in the upper region of the model is much more efficient in decelerating the stratospheric zonal flow than the external mode resonated here.

Fig. 4 shows a series of 525 mb geopotential height maps, at 5 day intervals from $t = 0$ to

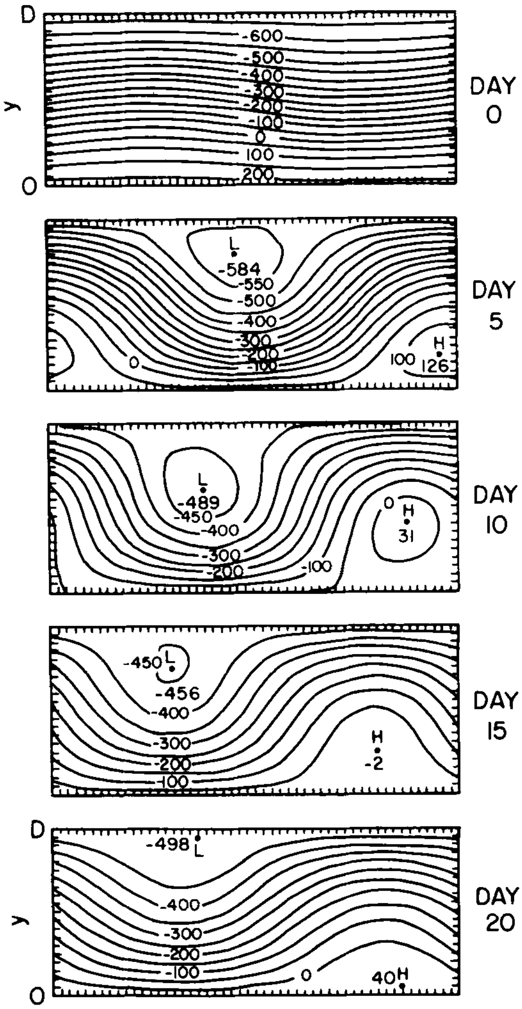

Fig. 4. The 525 mb height field (m) for the nonlinear integration, at five-day intervals from $t = 0$ (top) to $t = 20$ days (bottom).

$t = 20$ days, from the fully nonlinear integration. Because of the periodicity of the fields, only half of the zonal extent of the domain is presented. The maps show the establishment of a large amplitude stationary long wave whose finite-amplitude nature is quite evident, in particular from the closed contours which are present from day 5 to day 15. The topographic structure given by (3) is such that $h(x, y)$ has a zonal wavelength of $L/2$, with maxima at $x = L/8$ and $5L/8$, where L is the length of the channel. The maxima in the 525 mb height field are then seen first to develop about one quarter of a wavelength to the west of the topographic maxima and then to move westward. The maximum amplitude occurs at about $t = 7.5$ days (not shown). By day 15 the height wave is nearly half a wavelength to the west of the topographic wave and decaying. We see that the flow is quite clearly dominated by zonal wavenumber 2, as already mentioned. The higher harmonics slightly modify the flow so that, for example, the closed lows and highs are not quite symmetric in x.

A number of authors, such as Edmon et al. (1980) and Palmer (1981, 1982) have demonstrated that the Eliassen–Palm (EP) flux field and its divergence can be very useful diagnostic quantities in studies of wave–mean flow interaction. We will present here some EP cross-sections to illustrate the interaction of our forced disturbance with the mean zonal flow. The reader is referred to the above authors for a more thorough presentation of the concepts and for the details which have been omitted from this presentation.

From the nonlinear quasi-geostrophic equations it is possible to derive the following tendency equations for the mean zonal potential vorticity $\bar{q}$ and the mean zonal velocity component:

$$\frac{\partial \bar{q}}{\partial t} = -(\overline{v'q'})_y + \overline{D}_q = -(\nabla\cdot\boldsymbol{F})_y + \overline{D}_q \tag{6}$$

$$\frac{\partial \bar{u}}{\partial t} = \nabla\cdot\boldsymbol{F} + f\bar{v}^* + \overline{D}_u, \tag{7}$$

where

$$\boldsymbol{F} = (-\overline{u'v'}, f_0\overline{v'\phi'_Z}/N^2), \tag{8a}$$

$$\nabla\cdot\boldsymbol{F} = (-\overline{u'v'})_y + \rho_0^{-1}(\rho_0 f_0\overline{v'\phi'_Z}/N^2)_Z \tag{8b}$$

$$\bar{v}^* = \bar{v} - \rho_0^{-1}(\rho_0\overline{v'\phi'_Z}/N^2)_Z, \tag{9}$$

$\boldsymbol{F}$ being the EP flux vector, $\bar{v}^*$ the "residual" meridional circulation and $\overline{D}_q$ and $\overline{D}_u$ the appropriate dissipation terms. From the linearized potential vorticity equation one obtains

$$\frac{\partial A}{\partial t} = -\nabla\cdot\boldsymbol{F} + D_A, \tag{10}$$

where

$$A = (\overline{q'^2})/(2\bar{q}_y)$$

is the density of "EP wave activity" (Edmon et al., 1980) and D_A represents the dissipation of A. It is clear from (6) that in the absence of dissipation the divergence of $\boldsymbol{F}$ contains all the information on the eddy forcing of $\bar{q}$. From (10) we find that steady ($\partial A/\partial t = 0$) inviscid small-amplitude disturbances have $\nabla\cdot\boldsymbol{F} = 0$. This in turn implies through (7) that in the limit of inviscid steady linear flow $\bar{v}^*$ vanishes; in other words, a nonzero $\bar{v}^*$ is indicative of a violation of these conditions. In the present study, the waves do not necessarily have small amplitudes and the flow is not inviscid, which means that the three terms on the right-hand side of (7) can contribute to modifying the mean zonal wind. Palmer (1981) used EP cross-sections, showing $\boldsymbol{F}$ and its divergence, to discuss the evolution of a sudden stratospheric warming. In that case, even though the waves (mainly zonal wavenumber 2) had finite amplitudes and were not steady, $\nabla\cdot\boldsymbol{F}$ correlated well with the observed $\partial\bar{u}/\partial t$. We have therefore decided to use EP cross-sections to describe the interaction between the forced wave and the zonal flow.

EP cross-sections have been computed at various times during the nonlinear integration. On the diagrams, the y and Z components of $\boldsymbol{F}$ were scaled in the same way as the y and Z axes themselves so as to have an accurate representation of the vector directions, and the vector lengths were normalized by setting the length of the longest vector equal to the distance between neighbouring grid points.

The central panels of Fig. 5 show the EP cross-sections for the nonlinear integration after: (a) 10 days, (b) 20 days, (c) 22 days and (d) 26 days. Both the flux $\boldsymbol{F}$ and its divergence $\nabla\cdot\boldsymbol{F}$ are shown. The left-hand panels show the corresponding cross-sections for $\partial\bar{u}/\partial t$ and the right-hand panels those for the sum of the last two terms on the right of (7). The upward propaga-

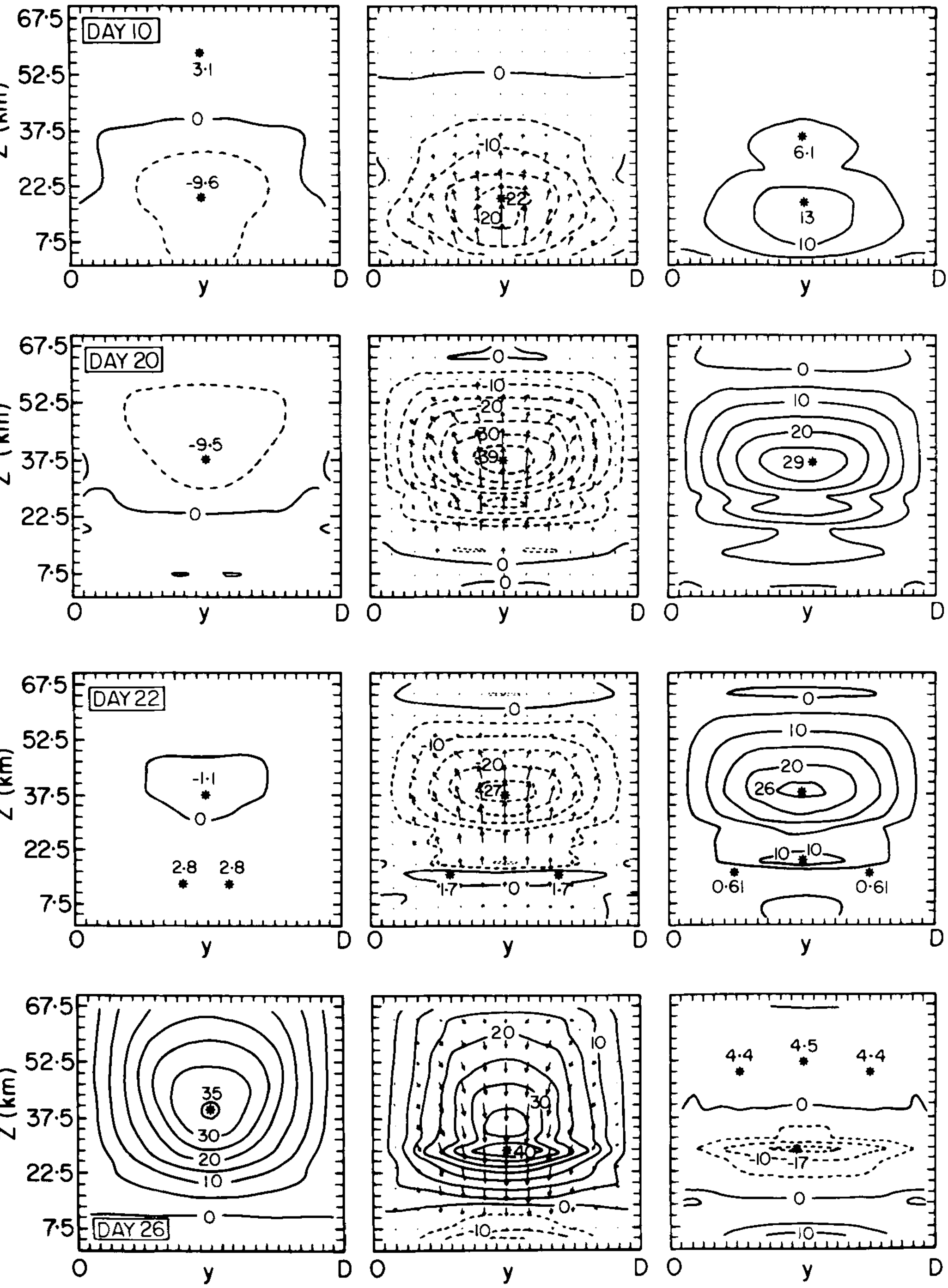

Fig. 5. Left-hand panels: $\partial \bar{u}/\partial t$ at $t = 10$, 20, 22 and 26 days as a function of Z and y, in units of 10^{-6} m/s^2 (or 0.0864 m s^{-1} day^{-1}). Centre panels: the vectors are those of the EP flux field $\boldsymbol{F}$ and the contours are those of $\nabla \cdot \boldsymbol{F}$, in the same units as $\partial \bar{u}/\partial t$. Right-hand panels: contours of the sum of the last two terms in (7).

tion of the wave at day 10 and 20 is evident. As seen from the contours of the central panels the flux is convergent over most of the domain, thus tending to decelerate the mean zonal wind. We can then expect that the mean zonal driving term would enter into play to restore the latter towards its value at $t = 0$. This is consistent with the right-hand panels which show a positive contribution to $\partial\bar{u}/\partial t$. The net effect, as seen from the left-hand panels, is a deceleration of $\bar{u}$ amounting to a maximum of about 10^{-5} m s^{-2} (0.9 m s^{-1} day^{-1}) at both day 10 and day 20. The net acceleration of $\bar{u}$ is seen to be well correlated with the term $\nabla \cdot \boldsymbol{F}$ but the sum of the residual circulation and the external forcing on $\bar{u}$ certainly plays an important role. On day 22, the flux vectors in the upper part of the model have a small downward component, suggesting that a reflection from the top boundary has taken place. Inspection of similar diagrams at other times (not shown) revealed that the first sign of a flux reversal near the upper boundary appears at day 21, much after the period of primary interest in this study. On day 26, the flux vectors all have a downward component and are divergent over most of the domain, thus acting to accelerate $\bar{u}$. We would then expect the latter to be returning towards its initial structure, implying a smaller restoring force $\bar{D}_u$ on the mean zonal wind. It is not too surprising then to see relatively small contributions to $\partial\bar{u}/\partial t$ on the right-hand panels.

5. Summary and conclusion

The primary motivation of this investigation was to extend the MD85 study of the first internal mode resonance by examining the resonance of the external mode. We particularly wished to investigate how long the resonant wave would continue to grow and how large it would become before the resonance condition was destroyed. Tung and Lindzen (1979) have previously examined the resonant growth of the external mode in a linear model having a uniform zonal wind and had obtained growth rates comparable to those in observed planetary wave amplification episodes. Using wind profiles having realistic horizontal and vertical shears and considering nonlinear effects, MD85 found much slower tropospheric growth rates in a model with topographic wave forcing. One major difference between the two studies was that while Tung and Lindzen had examined the resonance of the external mode, MD85 studied the resonance of an internal mode. The structure of the mean zonal wind used in MD85 was such that an external mode resonance could only be produced with unrealistically large zonal winds. In this paper, the zonal wind profile had realistic horizontal and vertical shears, as in MD85, but a uniform constant term was added; the important consequence was that resonance of the external mode could occur for more realistic zonal wind velocities.

A steady-state model was first used to find specific zonal wind profiles that made the external mode resonant. Some of these had realistic horizontal and vertical shears, as well as realistic tropospheric and stratospheric velocities. The external mode response of the linear version of our model was found to be rather insensitive to the stratospheric mean zonal velocities, in agreement with Salby (1981).

Linear time integrations were performed to obtain the wave growth rate in the absence of interactions with the mean zonal wind. The zonal flow was kept fixed, its structure chosen from among the realistic resonant wind profiles found in the steady-state experiments. When damping was included, the resonant wave grew by almost 50 dam in 10 days and when an equilibrium between forcing and damping was reached, the resonant wave had grown to an amplitude of 55 dam in the troposphere. Both this growth rate and equilibrium amplitude agree quite well with those calculated by Tung and Lindzen (1979).

A nonlinear integration was then performed to see whether or not the interaction with the mean zonal wind would throw the latter off resonance so early as to prevent the growth of the disturbance to a substantial amplitude. It was found that the mean zonal flow remained close enough to resonance to allow the forced wave to reach such a large amplitude that closed circulations formed in the mid-troposphere. For example, at 10 km the forced wave reached an amplitude of 37 dam. This is to be contrasted to the experiments of MD85 in which the resonant internal mode produced a major stratospheric warming which prevented the growing wave from achieving an amplitude larger than 10 dam in the troposphere.

Eliassen–Palm cross-sections of the nonlinear integration were presented to illustrate the vertical propagation of the forced wave and its interaction with the mean zonal flow. Evidence of a spurious reflection at the top boundary was observed at about day 21, after the main period of interest in this study.

Mitchell and Derome (1983) have shown that when an external source of energy (diabatic heating) forces resonant waves, in certain circumstances, the latter can reach a finite-amplitude blocking-like structure before the mean zonal wind moves off resonance, thereby reducing the wave growth rate. In the present study, the wave must extract energy from the mean zonal wind to grow, and we could thus expect the resonant growth to be curbed much earlier. However, our numerical results show that even in these circumstances, it is indeed possible for an external planetary wave to grow to sufficiently large amplitude to produce closed circulations in the troposphere. Naturally, it is not possible from the present study to conclude that resonance is necessarily at work during the rapid growth of planetary waves, but the results are consistent with such a possibility.

It should be kept in mind that topographic forcing is but one of the mechanisms which can lead to the growth of a planetary wave. It is probable that other mechanisms, such as land–sea thermal contrasts and transient eddy forcing, play a fundamental role in the genesis and maintenance of anomalous large amplitude planetary waves. What the present study has shown is that even in adverse conditions, when the wave energy is extracted from the zonal flow, the wave amplification can be substantial.

Some limitations of our model should be kept in mind. Our neglect of the tropospheric jet, for example, distorts the vertical structure of the resonant modes. In addition, the beta-plane approximation not only produces a distortion of the true geometry but, because of the side walls, promotes the growth of the forced disturbance by confining the energy horizontally. It would therefore be of interest to extend this work with a spherical geometry model and a more realistic representation of the earth's orography. It would also be instructive to perform experiments with other types of forcing, such as the time-averaged potential vorticity forcing due to the transient eddies, as obtained from atmospheric data. We can expect that the forcing will then be more localized in longitude. Mitchell and Derome (1983) have shown that a fairly localized forcing can still lead to considerable wave growth in a nonlinear beta-plane model when the initial basic state is resonant to one of the forced harmonics, but this type of experiment remains to be done in a spherical domain.

6. Acknowledgements

This research was supported by the Atmospheric Environment Service and the Natural Sciences and Engineering Research Council of Canada. The first author also benefited from a scholarship from the Fonds pour la formation de chercheurs et l'aide à la recherche of the Province of Québec. The authors would like to thank Ms. U. Seidenfuss for her help with the diagrams.

REFERENCES

Austin, J. F. 1980. The blocking of middle latitude westerly winds by planetary waves. *Q. J. R. Meteorol. Soc.* *106*, 327–350.

Edmon, H. J. Jr., Hoskins, B. J. and McIntyre, M. E. 1980. Eliassen–Palm cross sections for the troposphere. *J. Atmos. Sci.* *37*, 2600–2616.

Hansen, A. R. 1986. Observational characteristics of atmospheric planetary waves with bimodal amplitude distributions. In: *Anomalous atmospheric flows and blocking. Advances in Geophysics.* Academic Press, eds. B. Saltzman, R. Benzi and A. Wiin-Nielsen, vol. *29*, 101–133.

Held, I. M. 1983. Stationary and quasi-stationary eddies in the extratropical troposphere: theory. In: *Large-scale dynamical processes in the atmosphere.* Academic Press, eds. B. Hoskins and R. Pearce, 127–168.

Holton, J. R. and Dunkerton, T. 1978. On the role of wave transience and dissipation in stratospheric mean flow vacillations. *J. Atmos. Sci.* *35*, 740–744.

Holton, J. R. and Mass, C. 1976. Stratospheric vacillation cycles. *J. Atmos. Sci.* *33*, 2218–2225.

Kasahara, A. 1980. Effect of zonal flows on the free oscillations of a barotropic atmosphere. *J. Atmos. Sci.* *37*, 917–929.

Kusunoki, S. 1984. The response of a barotropic model atmosphere with realistic topography and a possibility of multiplicity of stationary solution. *J. Meteorol. Soc. Japan 62*, 583–596.

Matsuno, T. 1971. A dynamical model of the sudden stratospheric warming. *J. Atmos. Sci. 28*, 1479–1494.

Mitchell, H. L. 1982. Resonance of stationary waves in a model atmosphere. Ph.D. thesis, McGill University, 220 pp. [Available as Rep. 125, Dept. of Meteor., McGill University].

Mitchell, H. L. and Derome, J. 1983. Blocking-like solutions of the potential vorticity equation: Their stability at equilibrium and growth at resonance. *J. Atmos. Sci. 40*, 2522–2536.

Mitchell, H. L. and Derome, J. 1985. Resonance of topographically forced waves in a quasi-geostrophic model. *J. Atmos. Sci. 42*, 1653–1666.

Palmer, T. N. 1981. Diagnostic study of a wavenumber-2 stratospheric sudden warming in a transformed Eulerian-mean formalism. *J. Atmos. Sci. 38*, 844–855.

Palmer, T. N. 1982. Properties of Eliassen–Palm flux for the planetary scale motion. *J. Atmos. Sci. 39*, 992–997.

Salby, M. L. 1981. Rossby normal modes in nonuniform background configurations. Part I: Simple fields. *J. Atmos. Sci. 38*, 1803–1826.

Sutera, A. 1986. Probability density distribution of large-scale atmospheric flow. In: *Anomalous atmospheric flows and blocking. Advances in Geophysics.* Academic Press, eds. B. Saltzman, R. Benzi and A. Wiin-Nielsen, vol. *29*, 227–249.

Tung, K. K. and Lindzen, R. S. 1979. A theory of stationary long waves. Part I: A simple theory of blocking. *Mon. Wea. Rev. 107*, 714–734.